

## **Synthesis of water-soluble, highly branched arborescent poly(acrylate)s: a colloid-macromolecule chimera**

Jonas Quandt,<sup>a,b</sup> Rustam A. Gumerov,<sup>a,c</sup> Timon Kratzenberg,<sup>d</sup> Max Hohenschutz,<sup>d</sup> David Kulczycki,<sup>a,b</sup> Walter Richtering,<sup>d</sup> Igor I. Potemkin,<sup>a,c</sup> and Cesar Rodriguez-Emmenegger<sup>\*a,e,f,g</sup>

<sup>a</sup> DWI – Leibniz Institute for Interactive Materials, Forckenbeckstraße 50, 52074 Aachen, Germany

<sup>b</sup> Institute of Technical and Macromolecular Chemistry, RWTH Aachen University, Worringerweg 2, 52074 Aachen, Germany

<sup>c</sup> Physics Department, Lomonosov Moscow State University, Leninskie Gory 1-2, 119991 Moscow, Russian Federation

<sup>d</sup> Institute of Physical Chemistry, RWTH Aachen University, Landoltweg 2, 52056 Aachen, Germany, European Union

<sup>e</sup> Institute for Bioengineering of Catalonia (IBEC), The Barcelona Institute of Science and Technology, Carrer de Baldori Reixac, 10, 12, 08028 Barcelona, Spain.

<sup>f</sup> Institució Catalana de Recerca i Estudis Avançats (ICREA), Passeig Lluís Companys 23, 08010 Barcelona, Spain

<sup>g</sup> Biomedical Research Networking Center in Bioengineering Biomaterials and Nanomedicine, The Institute of Health Carlos III, 28029, Madrid, Spain

\*E-Mail: [crodriguez@ibecbarcelona.eu](mailto:crodriguez@ibecbarcelona.eu)

## 1. Materials and Methods

*Materials:* All reagents were used as received unless stated otherwise. 1,3,5-trioxane (99.9%), 2-bromopropionyl bromide (97%), 2-hydroxyethyl acrylate (HEA, 96%), 4-dimethylaminopyridine, 4-methoxyphenol (99% MEHQ), aluminum oxide 90 (active basic), copper(II) bromide (98%), dimethyl sulfoxide ( $\geq 99\%$ ), dimethyl sulfoxide- $d_6$  (99.9 atom % D), hexadecane (99%, reagent plus), hydrazine monohydrate (64-65%, reagent grade), Me6TREN (97%), methyl 2-bromopropionate (98%), oligo(ethylene glycol) methyl ether acrylate ( $M_n = 480$ ), and triethylamine (99.5%) were obtained from Sigma-Aldrich/ Merck KGaA (Darmstadt, Germany). 2-[2-(2-methoxyethoxy)ethoxy]ethyl acrylate ( $\geq 90\%$ , TEGMEA) was obtained from TCI Deutschland GmbH (Eschborn, Germany). Copper wire (99.9%,  $d = 0.0812$  cm) was obtained from Alfa Aesar (Kandel, Germany). Acetone (99.9%), dichloromethane (99.8%), methanol (99.8%, anhydrous) and tetrahydrofuran (99.5%, anhydrous) were obtained from Acros Organics (Geel, Belgium). Diethyl ether and heptane were obtained from Fisher Scientific GmbH (Schwerte, Germany). Deionized water was obtained from a Milli-Q-System from Merck Millipore. Cu(0)-wire was activated by hydrazine following the procedure described below. HEA was purified prior to the polymerization. A solution of 25 vol% HEA in water was prepared and extracted with heptane (6x) to remove residual diacrylates. The aqueous solution was saturated with NaCl and extracted with diethyl ether. The organic phase was dried with calcium sulphate and the solvent was removed under reduced pressure. Afterwards MEHQ ( $\approx 800$  ppm) was added and the monomer was stored under inert gas atmosphere in the freezer and used within the next days. Prior to polymerization the inhibitor was removed from all monomers (HEA, TEGMEA, OEGMEA) using a column of basic aluminum oxide. Hexadecane was purified three times over a column of basic aluminum oxide prior to IFT pendant drop experiments.

*Nuclear magnetic resonance spectroscopy (NMR):* All synthesized compounds were characterized by recording their NMR spectra at room temperature using a Bruker Avance III 400 spectrometer. Spectral analysis was performed using MNova V.14.3.2. Chemical shifts ( $\delta$ ) are reported relative to the solvent residual peaks (DMSO- $d_6$ :  $\delta_H = 2.50$  ppm; D<sub>2</sub>O:  $\delta_H = 4.79$  ppm). The following abbreviations were used: s = singlet, d = doublet, t = triplet, q = quartet, dd = doublet of doublets, m = multiplet. Coupling constants ( $J$ ) are reported in Hz.

*Size exclusion chromatography (SEC):* SEC was performed under two different conditions. (A) SEC was conducted using tetrahydrofuran (THF,  $\geq 99.7\%$ , unstabilized, HiPerSolv CHROMANORM<sup>®</sup> HPLC grade, VWR) as the eluent at  $1.0 \text{ mL}\cdot\text{min}^{-1}$  and  $20 \text{ }^\circ\text{C}$ . The system included an HPLC pump (1260 Infinity II, Agilent), a refractive index detector (RI) (1290 Infinity II, Agilent), and a multi-angle laser light scattering (MALLS) detector (SLD 7100, Polymer Standards Service). A pre-column ( $8\times 50 \text{ mm}$ ) and four SDplus gel columns ( $8\times 300 \text{ mm}$ , MZ Analysentechnik) with  $5 \text{ }\mu\text{m}$  particle diameters and nominal pore sizes of 50, 102,  $10^3$ , and  $10^4 \text{ \AA}$  were used. As an internal standard, samples contained  $250 \text{ mg}\cdot\text{L}^{-1}$  3,5-di-tert-4-butylhydroxytoluene (BHT,  $\geq 99\%$ , Fluka). Calibration was performed using narrow-distribution PMMA standards (Polymer Standards Service). (B) SEC was conducted using dimethylformamide (DMF,  $\geq 99.9\%$ , HiPerSolv CHROMANORM<sup>®</sup> HPLC grade, VWR) as the eluent with  $1 \text{ g}\cdot\text{L}^{-1}$  LiBr ( $\geq 99\%$ , Sigma-Aldrich). The system comprised an HPLC pump (1260 Infinity, Agilent) and a refractive index detector (RI) (1260 Infinity II, Agilent). Samples were prepared with  $2 \text{ }\mu\text{L}\cdot\text{mL}^{-1}$  toluene ( $\geq 99\%$ , Sigma-Aldrich) as an internal standard. Separation was achieved using one pre-column ( $8\times 50 \text{ mm}$ ) and three GRAM gel columns ( $8\times 300 \text{ mm}$ , Polymer Standards Service) with a  $10 \text{ }\mu\text{m}$  particle diameter and nominal pore sizes of 30, 1000, and  $1000 \text{ \AA}$ . The flow rate was  $1.0 \text{ mL}\cdot\text{min}^{-1}$  at  $60 \text{ }^\circ\text{C}$ . Calibration was performed using narrow-distribution poly(methyl methacrylate) (PMMA) standards (Polymer Standards Service). Data analysis was carried out using PSS WinGPC UniChrom software (Version 8.3.2)

*Dynamic Light Scattering (DLS):* DLS was used to determine the hydrodynamic radius ( $R_h$ ) of arborescent polymers in dilute solution in water and tetrahydrofuran. Measurements were carried out using a Zetasizer Ultra (Malvern Instruments) with a fixed scattering angle of  $\vartheta = 90^\circ$ , a laser operating at  $\lambda = 632.8 \text{ nm}$ . Prior to each measurement, samples were equilibrated at  $25 \text{ }^\circ\text{C}$  for 90 seconds. Multiple acquisitions ( $\geq 10$ ) were performed for each sample. Data processing was conducted using the instrument's ZS XPLOER software (Version 1.2.0.91).

*Static Light Scattering (SLS):* Static light scattering was used to determine the molar mass  $M_w$ , the second virial coefficient  $A_2$  and the radius of gyration  $R_G$  of G3 poly(TEGMEA-co-HEA) in water and tetrahydrofuran. Samples with concentrations between  $0.05$  and  $1 \text{ mg}\cdot\text{mL}^{-1}$  were measured on a SLS-

Systemtechnik GmbH instrument equipped with a laser ( $\lambda = 642 \text{ nm}$ ) and a toluene bath at  $T = 25 \text{ }^\circ\text{C}$ . The scattering intensity was measured between  $30^\circ$  and  $150^\circ$  in steps of  $10^\circ$  and is expressed as the Rayleigh ratio by use of toluene as an absolute scattering standard. The Rayleigh ratios were ensured to lie within the Guinier regime ( $R_G q < 1$ ) and were doubly extrapolated to momentum transfer  $q = 0$  and concentration  $c = 0$  in a Zimm plot according to the Zimm equation:

$$\frac{Kc}{R} = \frac{1}{M_W}(1 + q^2 R_G^2) + 2A_2 c \quad (1)$$

With  $K = \frac{4\pi^2 n_s^2}{N_A \lambda^4} \left(\frac{dn}{dc}\right)^2$  being the optical constant, where  $n_s$  is the refractive index of the solvent,  $N_A$  the Avogadro constant, and  $dn/dc$  the refractive index increment of the polymer.

The refractive index increment was measured at  $25 \text{ }^\circ\text{C}$  respectively in THF and in water on a refractometer by SLS-Systemtechnik with a laser ( $\lambda = 641 \text{ nm}$ ) for 7 concentrations between  $0.1$  and  $5 \text{ mg}\cdot\text{mL}^{-1}$  yielding  $dn/dc = 0.083 \text{ mL}\cdot\text{g}^{-1}$  in THF and  $dn/dc = 0.128 \text{ mL}\cdot\text{g}^{-1}$  in water.

*Atomic force microscopy (AFM) image analysis:* Additional image analysis was performed using a custom-written MATLAB script (version 2023b) to determine the occupied area of surface adsorbed arborescent polymers. Individual particles were cropped from the AFM images and particle segmentation was performed using k-means clustering. Segments from each particle were combined and isolated from the rest of the image data for further calculation. Consequently, the particle area could be calculated from the number of pixels assigned to the particle  $N_{\text{pixel}}$

and pixel area  $a_{\text{pixel}}$  according to the following equation:

$$A_{\text{particle}} = N_{\text{pixel}} \cdot a_{\text{pixel}} \quad (2)$$

*Dynamic interfacial tension:* Adsorption of arborescent polymer at the hexadecane-water interface was assessed by measuring the interfacial tension using the pendant drop analysis (DSA100, Krüss, Germany) as described in the literature.<sup>1,2</sup> A  $20 \mu\text{L}$  drop of arborescent polymer in water ( $G0$ - $G3$ ,  $1.5 \cdot 10^{-7} \text{ mmol}\cdot\text{mL}^{-1}$ ) was formed at the tip of a capillary immersed in a cuvette filled with hexadecane. Prior to the measurement hexadecane was purified three times over column of basic aluminum oxide. The measurement principle is founded on the analysis of the drop shape, which is governed by the

interplay between interfacial tension and the gravitational force. Interfacial tension facilitates the formation of a spherical drop, whereas gravity tends to deform it into a non-spherical shape. This equilibrium between interfacial tension and gravitational forces can be quantitatively described through the application of the Young–Laplace equation as outlined below:

$$\Delta P = \gamma \left( \frac{1}{R_1} + \frac{1}{R_2} \right) \quad (3)$$

where  $\Delta P$  is the pressure difference across the drop interface,  $\gamma$  is the interfacial tension and  $R_1$  and  $R_2$  denote the principal radii of the drop. During the measurement the shape of the drop is captured by a camera attached to the instrument. A shape parameter ( $B$ ) is iteratively adjusted until the calculated drop shape aligns with the observed drop shape and  $B$  is utilized to determine the interfacial tension using the following equation:

$$\gamma = \frac{\Delta \rho \cdot g \cdot d^2}{B} \quad (4)$$

Where  $\Delta \rho$  is the difference of the density of the two phases,  $g$  is the gravitational acceleration and  $d$  is the diameter of the drop. As a consequence of the adsorption of the arborescent polymer at the interface the shape of the drop changes. The drop shape was recorded by the instrument (one image per 0.5 s) and the interfacial tension was extracted from the analysis of the drop shape and the density difference of the liquids using the image analysis software of the manufacturer.

### **Dissipative Particle Dynamics Simulations**

*Coarse-graining:* The implementation of the DPD approach lies in the explicit representation of all modelling species. Simulation systems contain up to ten types of DPD particles: water (type W), hexadecane (type O), THF (type T), the TEGMEA monomer consisting of EGMEA part (a hydrophobic backbone with a single ethylene glycol (EG) unit, type A) and the EG pending group (comprising two EG units and the methyl end group, type H), HEA monomers and the branching points (types B and C respectively), the thiophenol caps (type E), the bromine groups (type F), “air” (type G), and, finally, the solid wall beads (type S). The interactions between the beads are estimated through the Flory-Huggins (FH) parameters  $\chi_{ij}$  and most of them were calculated through Hansen solubility parameter<sup>3</sup>:

$$\chi_{ij} = \frac{\alpha v_{\text{ref}} \left( (\delta_i^d - \delta_j^d)^2 + 0.25(\delta_i^p - \delta_j^p)^2 + 0.25(\delta_i^h - \delta_j^h)^2 \right)}{k_B T} \quad (5)$$

where  $\alpha$  is a numerical coefficient usually taken as 0.6;<sup>4</sup>  $v_{\text{ref}}$  is the reference average volume of  $i^{\text{th}}$  and  $j^{\text{th}}$  beads;  $\delta^d$ ,  $\delta^p$ ,  $\delta^h$  are the dispersion, polar and hydrogen bonding Hansen solubility parameters (HSP), which were obtained from the literature (see Table S2 in the Supporting Information). To define the  $v_{\text{ref}}$ , we defined a water mapping number,  $N_m$ , so that each bead corresponded, on average, to  $N_m = 7$  water molecules which gives the scaling factor  $r_c = 0.86$  nm for the standard value of number density  $\rho = 3$ . Simultaneously, with such a  $v_{\text{ref}}$ , all the beads have a mass of 126 Da. Regarding the increased mutual repulsion of DPD beads,  $a_{ij} = 100$ , a following linear relation was used:<sup>5</sup>  $\chi_{ij} \approx 0.28(a_{ij} - a_{ii})$ . The resulting set of parameters can be found in Table S3. There, the interactions between water beads and the beads of types H and B were set as 101.3 ( $\chi_{HW} = \chi_{BW} \approx 0.36$ ) to ensure the hydrophilic (PEG-like) polymer conditions.<sup>6,7</sup> Furthermore, the interactions between A and W beads and C and W were reconsidered as mildly hydrophobic ( $\chi_{AW} \approx 2$  and  $\chi_{CW} \approx 1.5$ ) due to the presence of methyl acrylate and EG groups. Note, that in our previous work the  $\chi_{AW}$  value was set as three due to the inclusion of the methyl end group, while in the current work this group, as mentioned, was included into a separate bead of type H.

*Simulation systems:* All the simulations were performed using the open source software LAMMPS,<sup>8</sup> with an integration time step  $\Delta t = 0.02\tau$  ( $\tau$  is a characteristic timescale). Three types of simulation systems were considered. In the first type, a single arborescent macromolecule together with a single-component solvent was placed in a cubic simulation box with periodic boundary conditions and dimensions varying from  $L_x \times L_y \times L_z = 36 r_c \times 36 r_c \times 36 r_c$  (31.0 nm  $\times$  31.0 nm  $\times$  31.0 nm) to  $L_x \times L_y \times L_z = 100 r_c \times 100 r_c \times 100 r_c$  (86.0 nm  $\times$  86.0 nm  $\times$  86.0 nm) depending on polymer generation and the solvent type (either water or THF). In the second type, a single G2 or G3 polymer was placed in a simulation box with periodic boundary conditions and dimensions (in the case of G3)  $L_x \times L_y \times L_z = 140 r_c \times 140 r_c \times 50 r_c$  (120.4 nm  $\times$  120.4 nm  $\times$  120.4 nm) containing W and O beads taken in a 1:1 proportion. Then, the box was gradually resized to the dimensions  $L_x \times L_y \times L_z \approx 260 r_c \times 260 r_c \times 14.5 r_c$  (223.6 nm  $\times$  223.6 nm  $\times$  12.5 nm) upon macromolecule deformation at the interface (for G2 the box sizes changed from  $L_x \times L_y \times L_z = 100 r_c \times 100 r_c \times 50 r_c$  to  $L_x \times L_y \times L_z \approx 160 r_c \times 160 r_c \times 19.5 r_c$ ). In the third type, a single G2 or G3 polymer was placed in a simulation box with periodic boundary conditions in XY plane and dimensions  $L_x \times L_y \times L_z = 180 r_c \times$

180  $r_c \times 40 r_c$  (154.8 nm  $\times$  154.8 nm  $\times$  34.4 nm) containing a solid two-layered wall formed by S beads at the bottom of the box.<sup>9</sup> The surrounding solvent beads representing the “air” had a strongly repulsive interaction with all the remaining bead types ( $a_{Gi} = 200$ , see Table S3). In turn, the interactions between the polymer-forming beads and the surface were set as 81.5 (the parameter was chosen to attempt to match the height of surface-adsorbed G3 as in the AFM measurements) thus realizing the effective attraction. Initially, all the systems were equilibrated up to  $8 \times 10^6$  time steps. Then, the statistics were gathered for an additional  $2 \times 10^6$  steps by taking snapshots each  $5 \times 10^4$  steps.

*Data analysis:* The sizes of arborescent polymers were estimated through the time-averaged values gyration radius  $R_g$  and its radial  $R_r$  and normal  $R_z$  components (the latter were used only in the case of oil-water interface),  $R_g^2 = R_r^2 + R_z^2$ , and  $R_r^2 = R_x^2 + R_y^2$ . The components were calculated by the following formulas:

$$R_r^2 = \frac{1}{2N^2} \sum_{i,j}^N \left( (x_i - x_j)^2 + (y_i - y_j)^2 \right) \quad (6)$$

$$R_z^2 = \frac{1}{2N^2} \sum_{i,j}^N \left( (z_i - z_j)^2 \right), \quad (7)$$

In addition, for the direct comparison with experimental data, the hydrodynamic radius was calculated through the convex hull method.<sup>10</sup>

**Table S1.** Characteristics of TEGMEA-based arborescent copolymer models used in simulations.

Description	$M_w^{\text{DPD}}$ (kg·mol <sup>-1</sup> )	$N^a$	BP per branch	DP branch	$R_g^{\text{THF}}$ (nm) <sup>b</sup>	$R_g^{\text{water}}$ (nm) <sup>c</sup>
<b>Core</b>	10.84	86	5	45	-	-
<b>G0</b>	75.09	596	5	53	6.2	4.3
<b>G1</b>	371.19	2946	5	49	10.1	6.5
<b>G2</b>	1725.7	1369	5	45	16.0	9.8
<b>G3</b>	8655.69	6869	5	46	25.2	16.0

<sup>a</sup> Total number of beads comprising the single model of the arborescent macromolecule.

<sup>b,c</sup> Values of gyration radius in THF (b) and water (c) solutions



**Table S2.** Hansen solubility parameters used in the DPD simulations.

Substance	$\delta^d$	$\delta^p$	$\delta^h$
EGMEA (type A) <sup>a</sup>	15.9	4.9	8.8
HEA (type B) <sup>a</sup>	16.6	6.7	16.0
Branching point (type C) <sup>a</sup>	16.2	6.3	9.4
EG pending group (type H) <sup>b</sup>	17	10.0	5.0
Thiophenol end caps (type E) <sup>a</sup>	22.5	0.3	0.0
Bromine end group (type F) <sup>b</sup>	18.2	14.9	0
THF (type T) <sup>b</sup>	16.8	5.7	8
Hexadecane (type O) <sup>b</sup>	16.3	0	0
Water (type W) <sup>b</sup>	15.5	16	42.3

<sup>a</sup> Calculated using van Krevelen method<sup>1</sup>; <sup>b</sup> taken from Hansen's book<sup>2</sup>

**Table S3:** DPD interaction parameters (in units of  $k_B T/r_c$ ) used in the simulations. The numbers in brackets in the non-diagonal cells are the corresponding values of Flory-Huggins parameter.

$a_{ij}(\chi_{ij})$	A	B	C	H	E	F	T	O	W
A	100	101.5	100.1	101.2	107.4	105.4	100.1	102.8	107.0
B		100	101.2	103.6	111.9	106.3	101.8	108.2	101.3
C			100	101.0	107.8	104.9	100.1	103.5	105.4
H				100	106.6	101.5	100.4	103.5	101.3
E					100	107.8	106.1	104.2	161.0
F						100	106.4	104.3	149.7
T							100	- <sup>a</sup>	- <sup>a</sup>
O								100	155.9
W									100

<sup>a</sup> The interactions that were not considered both in experiments and simulations

## Synthesis

*Activation of Cu(0)-wire:* A 500 mL Schlenk flask was purged with argon and maintained under an inert atmosphere. A stirring bar wrapped with 2 m of Cu(0) wire (diameter = 0.0812 cm) was placed in the flask and suspended in the upper section using external magnets. Anhydrous DMSO (200 mL) and hydrazine monohydrate (31  $\mu$ L) were then added. After degassing by four freeze-pump-thaw cycles, the Cu(0) wire was submerged in the hydrazine/DMSO solution and stirred at room temperature for 45 min. To rinse the wire, the reaction mixture was replaced sequentially with 100 mL of dry methanol, followed by dry tetrahydrofuran. After the solvent was removed, the stirring bar and Cu(0) wire were dried under vacuum and stored in a nitrogen atmosphere inside a glove box.

*Kinetic analysis of homopolymerization:* Into a 25 mL Schlenk flask the respective monomer HEA, TEGMEA or OEGMEA (50 equiv., 17.281 mmol), internal standard (1,3,5-trioxane, 30 mg), Me<sub>6</sub>TREN (7.96 mg, 0.0346 mmol, 0.1 equiv.), copper (II) bromide (3.86 mg, 0.0173 mmol, 0.05 equiv.) and DMSO (5 mL) were added. The initiator methyl 2-bromopropionate (57.7 mg, 0.346 mmol, 1 equiv.) was added last and 100  $\mu$ L sample for NMR analysis was taken, before freezing the solution in liquid nitrogen. A hydrazine-activated Cu(0) wire (3.75 cm) was wrapped around a magnetic stirring bar and suspended over the frozen solution by an external magnet. The mixture was degassed using five freeze-pump-thaw cycles, and subsequently, the Schlenk flask was filled with argon following the final cycle. The reaction was initiated by transferring the flask into a water bath maintained at 35 °C and immersing the stirring bar into the solution at 750 rpm. The kinetic samples (100  $\mu$ L) for <sup>1</sup>H NMR spectroscopy and SEC were removed through a three-way valve under a countercurrent argon stream, utilizing a gastight syringe. To terminate the polymerization, the stirring bar with attached Cu(0) wire was removed using an external magnet, and the flask was exposed to oxygen. NMR samples were dissolved in deuterated DMSO to determine the conversion, and samples for SEC analysis were dissolved in THF (TEGMEA, OEGMEA) and DMF (HEA).

*Kinetic analysis of copolymerization:* The copolymerization followed the same protocol as described above for the homopolymerization. A monomer ratio of 90% TEGMEA and 10% HEA was used. The molar ratios were as follows:

*Backbone:* [TEGMEA]<sub>0</sub>/[HEA]<sub>0</sub>/[MBP]<sub>0</sub>/[CuBr<sub>2</sub>]<sub>0</sub>/[Me<sub>6</sub>TREN]<sub>0</sub> = 45/5/1/0.05/0.1,

n<sub>Monomer</sub> = 17.281 mmol, n<sub>MBP</sub> = 0.346 mmol, activated Cu<sup>0</sup>-wire (3.75 cm), V<sub>DMSO</sub> = 5 mL at 25 °C.

*Grafting-from:* [TEGMEA]<sub>0</sub>/[HEA]<sub>0</sub>/[MBP]<sub>0</sub>/[CuBr<sub>2</sub>]<sub>0</sub>/[Me<sub>6</sub>TREN]<sub>0</sub> = 180/20/1/0.05/0.1,

n<sub>Monomer</sub> = 69.1 mmol, n<sub>MBP</sub> = 0.346 mmol, activated Cu(0)-wire (15 cm), V<sub>DMSO</sub> = 20 mL at 25 °C.

*End-group capping with thiophenol:* The following amounts were used for the end-group capping described in the main manuscript.

*Backbone:* poly(TEGMEA-co-HEA) (1.12 mmol, 1 equiv.), TEA (171.0 mg, 1.69 mmol, 1.5 equiv.), thiophenol (186.2 mg, 1.69 mmol, 1.5 equiv.)

*G0-G2:* poly(TEGMEA-co-HEA) (0.346 mmol, 1 equiv.), TEA (52.4 mg, 0.52 mmol, 1.5 equiv.), thiophenol (57.1 mg, 0.52 mmol, 1.5 equiv.)

*G3:* TEA (28.5 mg, 0.25 mmol, 1.5 equiv.), thiophenol (57.1 mg, 0.25 mmol, 1.5 equiv.), added directly into the polymerization mixture

*Polymerization and transformation into the macroinitiator.*

Table S4 presents the polymer yield obtained after polymerization and after transformation into the corresponding macroinitiator for different arborescent generations. A decrease in the final macroinitiator yield with increasing generation is attributed to polymer loss during workup procedures, such as precipitation. As the generation increases, the polymer viscosity rises significantly, making redissolution increasingly challenging. Figure S6 compares the SEC elution profiles of the polymer immediately after polymerization and after macroinitiator formation, indicating that the molecular weight distribution remains unaffected by the workup procedures.

**Table S4:** Obtained yield for the different generation of arborescent polymer.

Generation	Conv. Polym. (%)	Polymerization		Macroinitiator	
		Mass (g)	Yield (%)	Mass	Yield
linear	89	12.4	95	10.8	83
G0	26	3.7	83	3.57	79
G1	24	3.9	84	3.1	67
G2	23	2.9	77	2.3	54
G3*	23	2.0	92	-	-
Overall yield (%)**					22

\*G3 after in-situ end group capping. Mass was determined gravimetrically from the G3 in DMSO solution after dialysis.

\*\*Overall yield was calculated as the product of yields of macroinitiators from linear to G2 and the yield after EGF for G3.

#### Summary <sup>1</sup>H-NMR arborescent macroinitiator

Backbone: <sup>1</sup>H-NMR (400 MHz, DMSO)  $\delta$ (ppm) 7.46 – 7.27 (m, 5H), 4.65 (t,  $J = 6.7$  Hz, 5H), 4.32 (s, 9H), 4.28 – 4.15 (m, 9H), 4.12 (s, 84H), 3.82 – 3.64 (m, 2H), 3.66 – 3.56 (m, 81H), 3.55 – 3.48 (m, 243H), 3.43 (dd,  $J = 5.9, 3.6$  Hz, 81H), 3.25 (s, 116H), 2.68 (s, 2H), 2.32 (d,  $J = 33.4$  Hz, 45H), 2.08 – 1.17 (m, 98H), 1.06 (p,  $J = 3.3$  Hz, 3H).

G0: <sup>1</sup>H-NMR (400 MHz, DMSO)  $\delta$ (ppm) 7.46 – 7.32 (m, 5H), 4.62 (q,  $J = 6.9$  Hz, 5H), 4.30 (s, 11H), 4.23 (s, 13H), 4.10 (s, 125H), 3.58 (d,  $J = 5.4$  Hz, 113H), 3.54 – 3.47 (m, 354H), 3.42 (dd,  $J = 6.0, 3.6$  Hz, 125H), 3.23 (s, 135H), 2.67 (s, 3H), 2.30 (d,  $J = 27.1$  Hz, 54H), 1.97 – 1.30 (m, 128H), 1.05 (s, 3H).

G1: <sup>1</sup>H-NMR (400 MHz, DMSO)  $\delta$ (ppm) 7.48 – 7.28 (m, 5H), 4.67 – 4.56 (m, 5H), 4.30 (s, 12H), 4.23 (s, 15H), 4.10 (s, 108H), 3.58 (d,  $J = 5.1$  Hz, 109H), 3.54 – 3.47 (m, 326H), 3.42 (dd,  $J = 6.1, 3.5$  Hz, 110H), 3.23 (s, 162H), 2.66 (s, 2H), 2.30 (d,  $J = 26.8$  Hz, 51H), 1.95 – 1.27 (m, 116H), 1.04 (s, 3H).

G2: <sup>1</sup>H-NMR (400 MHz, D<sub>2</sub>O)  $\delta$ (ppm) 7.43 – 7.34 (m, 5H), 4.67 – 4.56 (m, 5H), 4.27 (d, 19H), 4.18 – 3.99 (m, 102H), 3.58 (t,  $J = 4.6$  Hz, 91H), 3.55 – 3.45 (m, 265H), 3.42 (dd,  $J = 6.0, 3.6$  Hz, 94H), 3.24 (d,  $J = 4.2$  Hz, 142H), 2.66 (s, 2H), 2.27 (s, 48H), 1.96 – 1.19 (m, 118H), 1.04 (s, 3H).

G3\*: <sup>1</sup>H-NMR (400 MHz, DMSO)  $\delta$ (ppm) 7.39 (dd,  $J = 29.9, 5.6$  Hz, 5H), 4.65 (s, 4H), 4.36 – 3.86 (m, 101H), 3.58 (s, 129H), 3.50 (d,  $J = 6.2$  Hz, 231H), 3.42 (dd,  $J = 6.0, 3.5$  Hz, 93H), 3.23 (d,  $J = 3.9$  Hz, 114H), 2.69 (d,  $J = 17.9$  Hz, 2H), 2.27 (s, 43H), 1.69 (d,  $J = 82.2$  Hz, 85H), 1.05 (s, 3H).

For G3 the <sup>1</sup>H-NMR after end-group capping is reported.

## 2. Supplementary Results

### Kinetic analysis of water-soluble acrylate monomers

Figure S1 to S3 show the complete kinetic analysis for the homopolymerization of HEA, TEGMEA and OEGMEA shown in the main manuscript. For all three monomers both molecular weights determined from  $^1\text{H-NMR}$  and SEC showed a linear increase with the theoretical molecular weight. The initiation efficiency was high in the range from 92-95% (Figure S1B, S2B and S3B). The dispersity decreases during the polymerization to  $\bar{D} = 1.11$  for conversions above 30% with corresponding narrow and monomodal SEC-profiles. For OEGMEA the SEC-profiles show a slight tail formation at higher conversions.

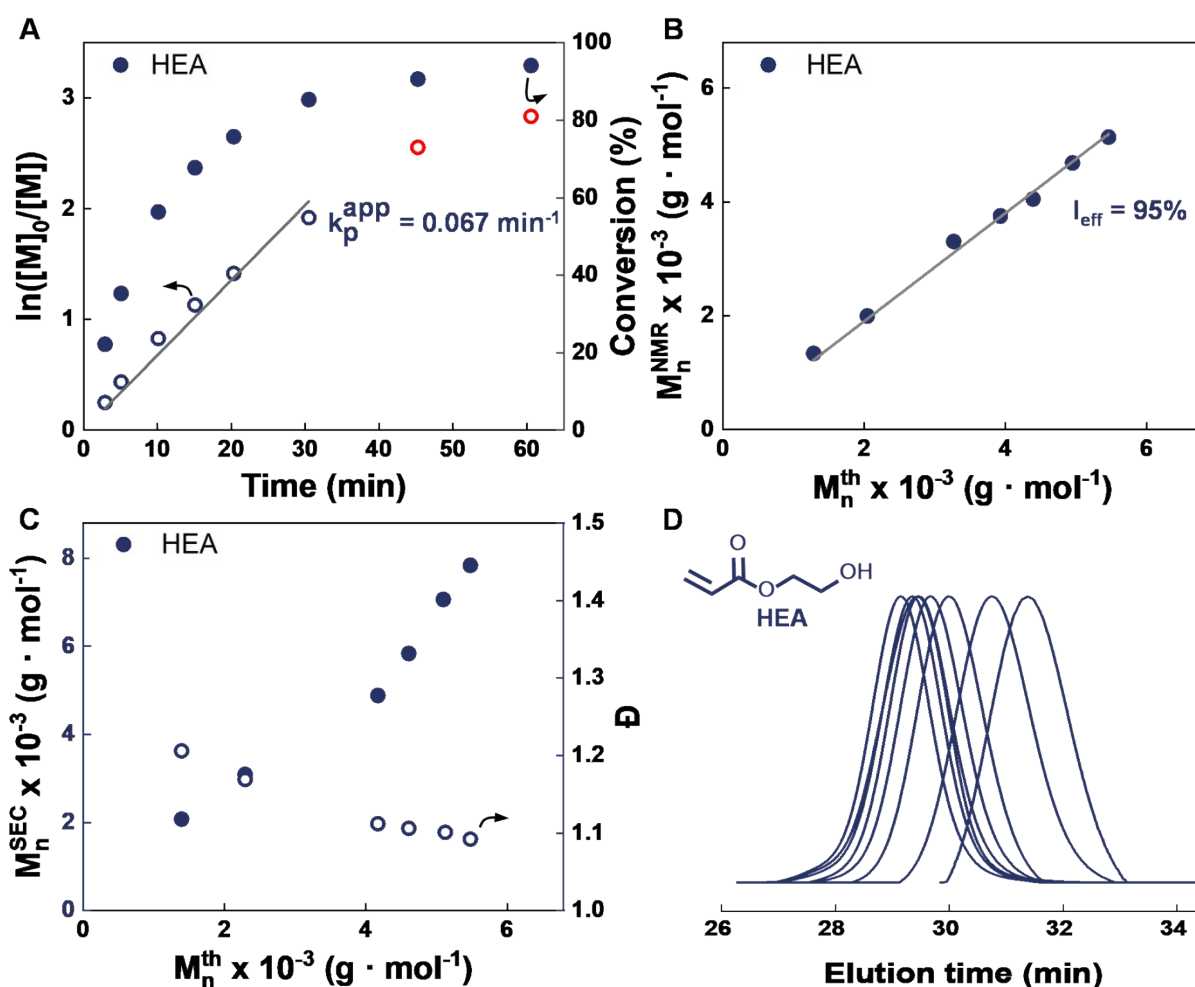


**Figure S1** Kinetic analysis of the homopolymerization of HEA: (A) conversion and semilogarithmic plot  $\ln([M]/[M]_0)$  with polymerization time (red data points excluded from the fit), (B) correlation of the molecular development calculated from NMR with the theoretical molecular weight, (C) development of dispersity and molecular weight from SEC in DMF with the theoretical molecular weight, (D) corresponding SEC-elugrams. Reaction conditions:  $[M]_0/[MBP]_0/[CuBr_2]_0/[Me_6TREN]_0 = 50/1/0.05/0.1$ ,  $n_{\text{Monomer}} = 17.281 \text{ mmol}$ ,  $n_{\text{MBP}} = 0.346 \text{ mmol}$ , activated Cu(0)-wire,  $V_{\text{DMSO}} = 5 \text{ mL}$  at  $35 \text{ }^\circ\text{C}$ .

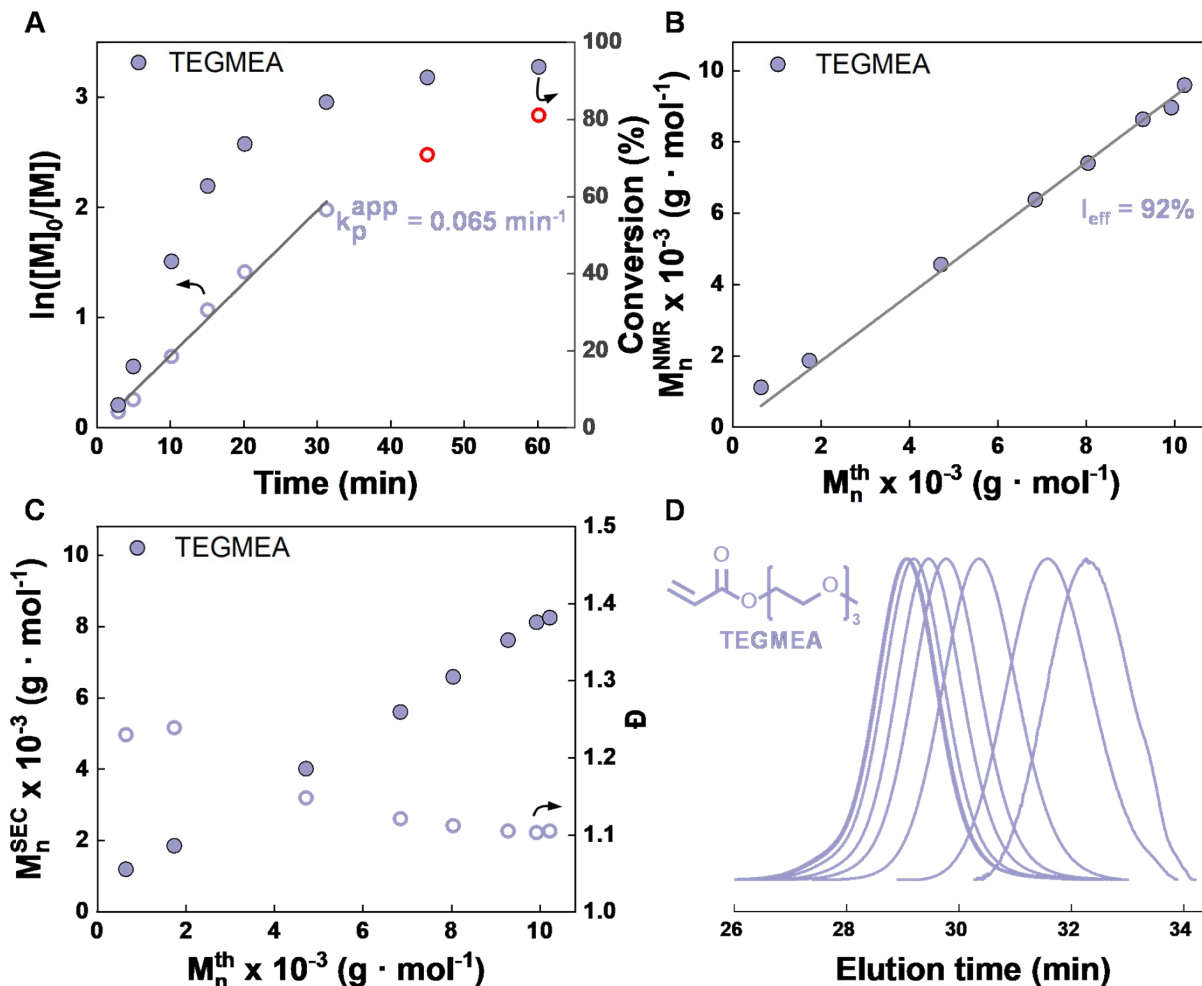


**Figure S2** Kinetic analysis of the homopolymerization of TEGMEA: (A) conversion and semilogarithmic plot  $\ln([M]/[M]_0)$  with polymerization time (red data points excluded from the fit) (B) correlation of the molecular development calculated from NMR with the theoretical molecular weight, (C) development of dispersity and molecular weight from SEC in THF with the theoretical molecular weight, (D) corresponding SEC-elugrams. Reaction conditions:  $[M]_0/[MBP]_0/[CuBr_2]_0/[Me_6TREN]_0 = 50/1/0.05/0.1$ ,  $n_{Monomer} = 17.281 \text{ mmol}$ ,  $n_{MBP} = 0.346 \text{ mmol}$ , activated Cu(0)-wire,  $V_{DMSO} = 5 \text{ mL}$  at  $35 \text{ }^\circ\text{C}$ .

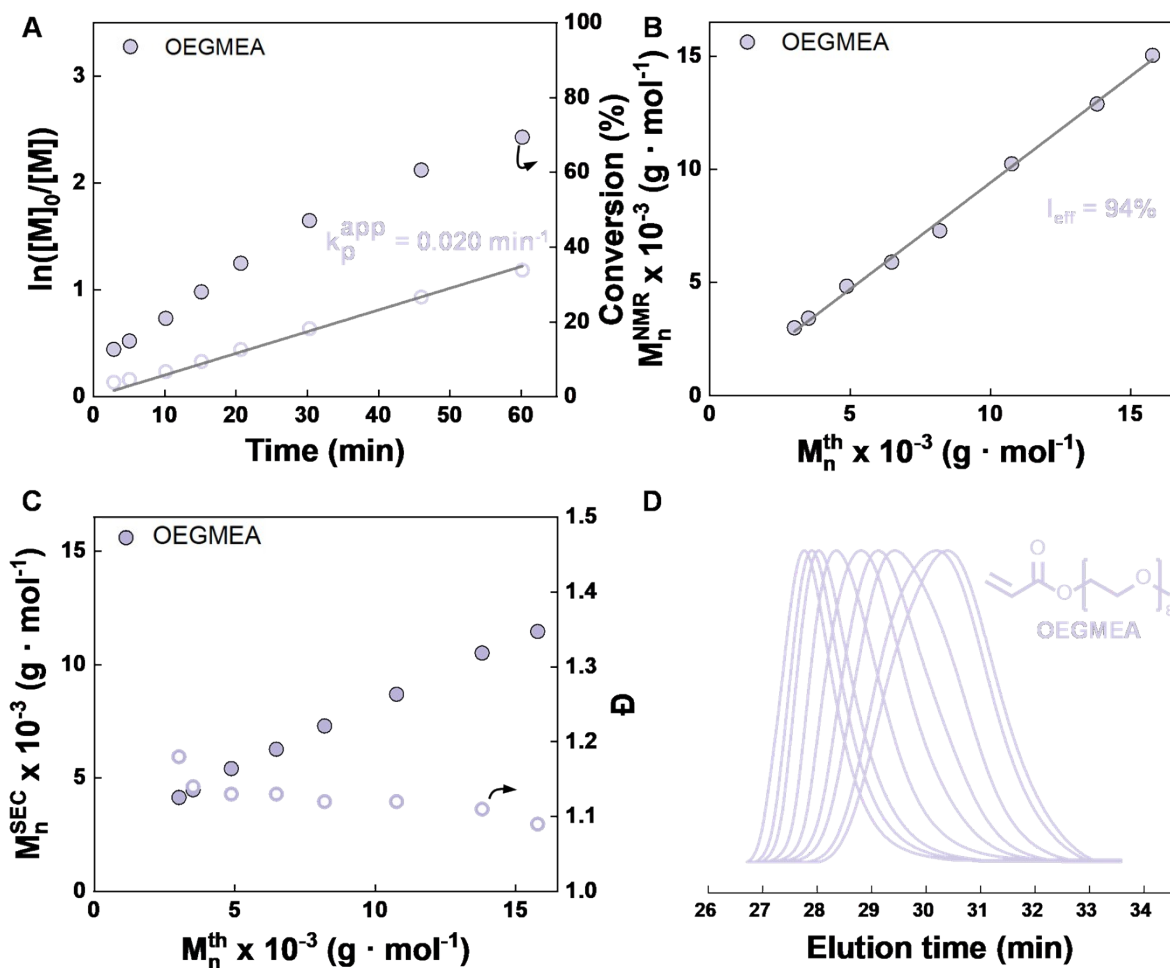


**Figure S3** Kinetic analysis of the homopolymerization of OEGMEA: (A) conversion and semilogarithmic plot  $\ln([M]/[M]_0)$  with polymerization time (red data points excluded from the fit), (B) correlation of the molecular weight development calculated from NMR with the theoretical molecular weight, (C) development of dispersity and molecular weight from SEC in THF with the theoretical molecular weight, (D) corresponding SEC-elugrams. Reaction conditions:  $[M]_0/[MBP]_0/[CuBr_2]_0/[Me_6TREN]_0 = 50/1/0.05/0.1$ ,  $n_{Monomer} = 17.281 \text{ mmol}$ ,  $n_{MBP} = 0.346 \text{ mmol}$ , activated Cu(0)-wire,  $V_{DMSO} = 5 \text{ mL}$  at  $35 \text{ }^\circ\text{C}$ .

## Grafting of arborescent polymers

### Calculation of the theoretical molecular weight

For the calculation of the theoretical molecular weight we first considered the number of initiating sites  $I_p$  of a generation  $G$  as:

$$I_p = I_{p-1} \cdot b \cdot DP_p \quad (8)$$

Herein  $p$  denotes the number of grafting-from polymerization performed ( $p \equiv G - 1$ ; backbone  $p = 0$ ,  $G0$   $p = 1$ ).  $b$  is the fraction of HEA functionalized with new initiator groups that will serve as branching points.  $DP_p$  is the degree of polymerization in the respective grafting step  $p$ . Therefore, with  $p = 0$  for the linear backbone  $I_0 = b \cdot DP_0$  and with  $p = 1$  for generation 0  $I_1 = I_0 \cdot b \cdot DP_0$  follows:

$$I_1 = b^2 \cdot DP_0 \cdot DP_1 \quad (9)$$

and the equation progresses as:

$$I_p = b^{p+1} \cdot \prod_{k=-1}^p DP_k \quad (10)$$

In the next step the total number of repeating units per generation  $R_p$  is considered

$$R_p = I_{p-1} \cdot DP_p \quad (11)$$

To obtain the total number of repeating units of an arborescent polymer the summation over all grafting generations is performed.

$$R_p = \sum_{j=0}^p I_{j-1} \cdot DP_j = \sum_{j=0}^p DP_j \cdot (b^j \cdot \prod_{k=-1}^{j-1} DP_k) = \sum_{j=0}^p (b^j \cdot \prod_{k=-1}^j DP_k) \quad (12)$$

and multiplied with the molecular weight of the repeating units  $M_R$ .

$$M = M_R \cdot \left[ \sum_{j=0}^p (b^j \cdot \prod_{k=-1}^j DP_k) \right] \quad (13)$$

For the copolymer of TEGMEA and HEA  $M_R = M_{HEA} \cdot r_1 + M_{TEGMEA} \cdot r_2$  where  $r_1$  and  $r_2$  denote the respective ratio of the monomer. In the last step we considered, that the molecular weight of the end groups is different from the repeating units. Each graft has two end groups, the former initiator and the chain end, and the number of end groups is twice the number of initiating sites of the previous

generation. If we consider  $M_E$  as the summation of the molecular weight of the two end groups the theoretical molecular weight can be calculated as:

$$M_n^{th} = M_R \cdot \left[ \sum_{j=0}^p (b^j \cdot \prod_{k=-1}^j DP_k) \right] + M_E \cdot \left[ \sum_{j=0}^p (2b^j \cdot \prod_{k=-1}^{j-1} DP_k) \right] \quad (14)$$

#### *Characterization of the linear macroinitiator poly(TEGMEA-co-HEA) by NMR*

Figure S4 shows the 1H-NMR of the linear macroinitiator poly(TEGMEA-co-HEA) (Table 1, entry 1, main manuscript) in DMSO-d<sub>6</sub> used to characterize the DP of the grafts, the end-group functionality (EGF) and the degree of functionalization with new initiator groups. For all calculations, the integral of the methyl group of the initiator (**3**, 3H) was set to correspond to 3 protons. The *DP* was determined by comparing the integral of the same methyl signal (**3**, 3H) and the -CH-group of the backbone (**5,5'**, 1H), which results in a *DP* = 45. The EGF was determined by comparing the integral of the thiophenol end groups (**15**, 5H), with the maximum integral value of 5H, which represents 100% EGF, using the following formula.

$$EGF = \frac{I_{15}}{5} \quad (15)$$

Leading to an EGF >98% for the linear backbone. From the ratio of newly introduced initiating sites  $I_P$  is calculated by

$$I_P = \frac{I_{16}}{I_{5,5'}} \quad (16)$$

demonstrating that the amount of HEA functionalized with initiator groups is at 10%.

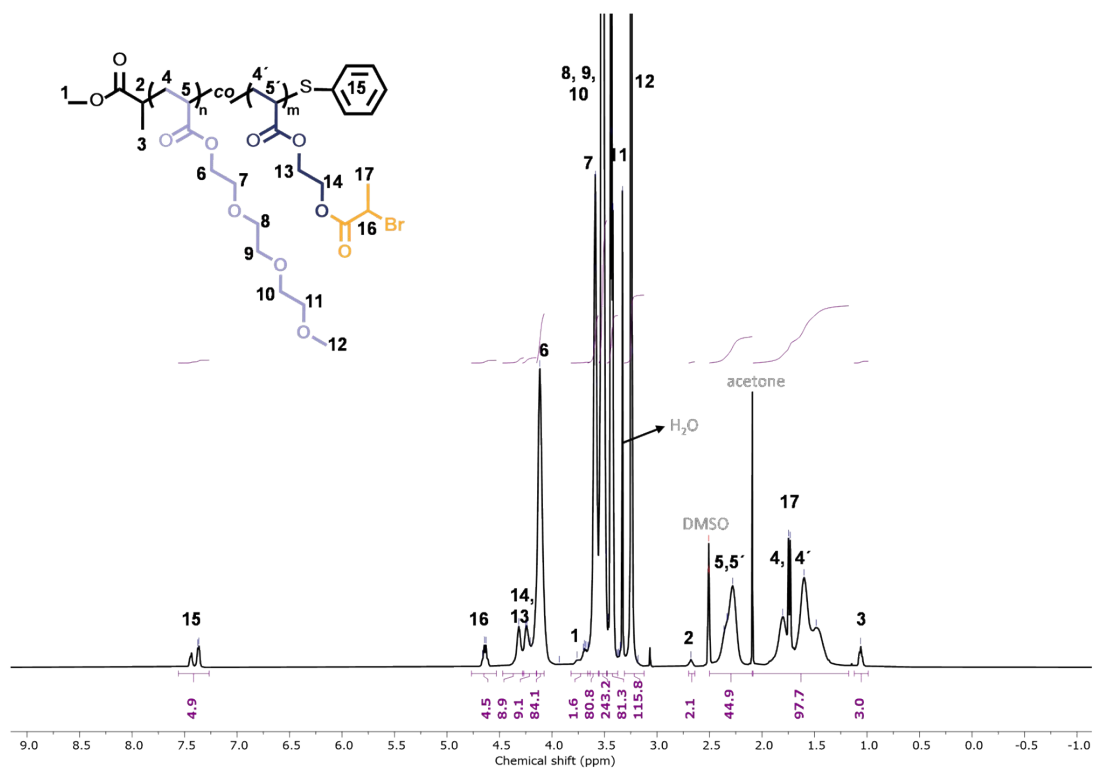


Figure S4.  $^1\text{H-NMR}$  of linear poly(TEGMEA-co-HEA) with  $DP = 45$ ,  $M_n^{SEC} = 9.6 \text{ kg}\cdot\text{mol}^{-1}$  and  $\mathcal{D} = 1.09$ .

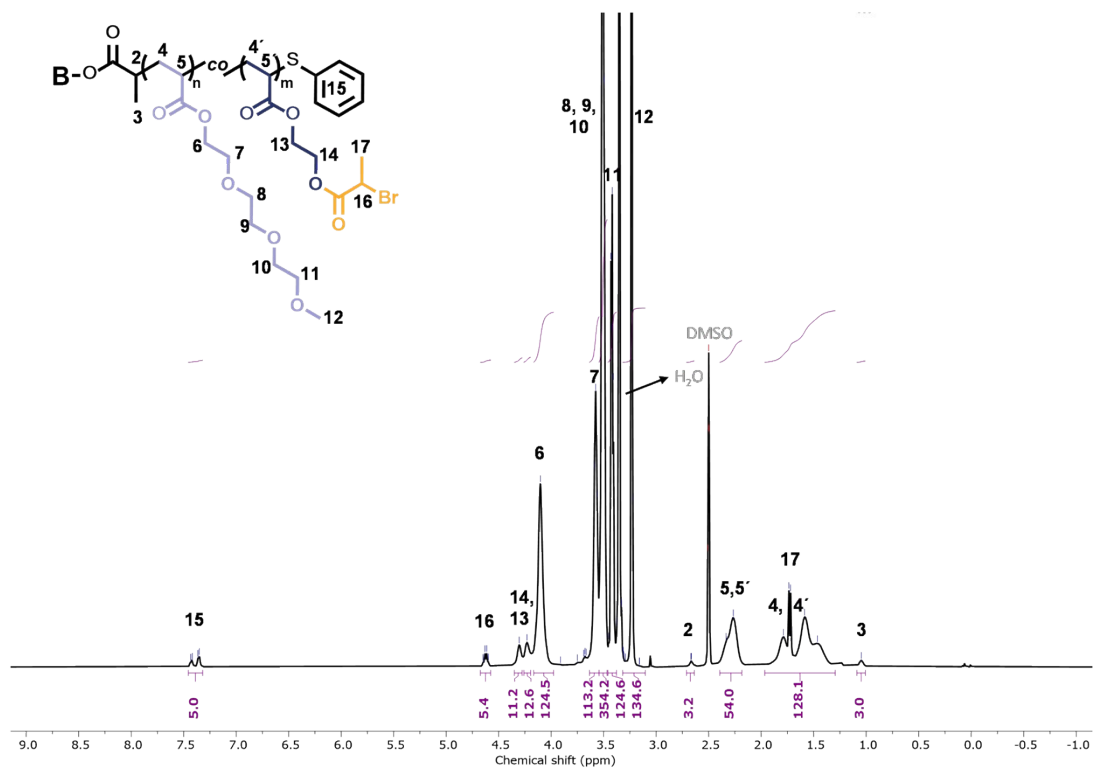


Figure S5.  $^1\text{H-NMR}$  of G0-poly(TEGMEA-co-HEA) with  $DP = 53$ ,  $M_w^{SLS} = 60 \text{ kg}\cdot\text{mol}^{-1}$  and  $\mathcal{D} = 1.09$ .

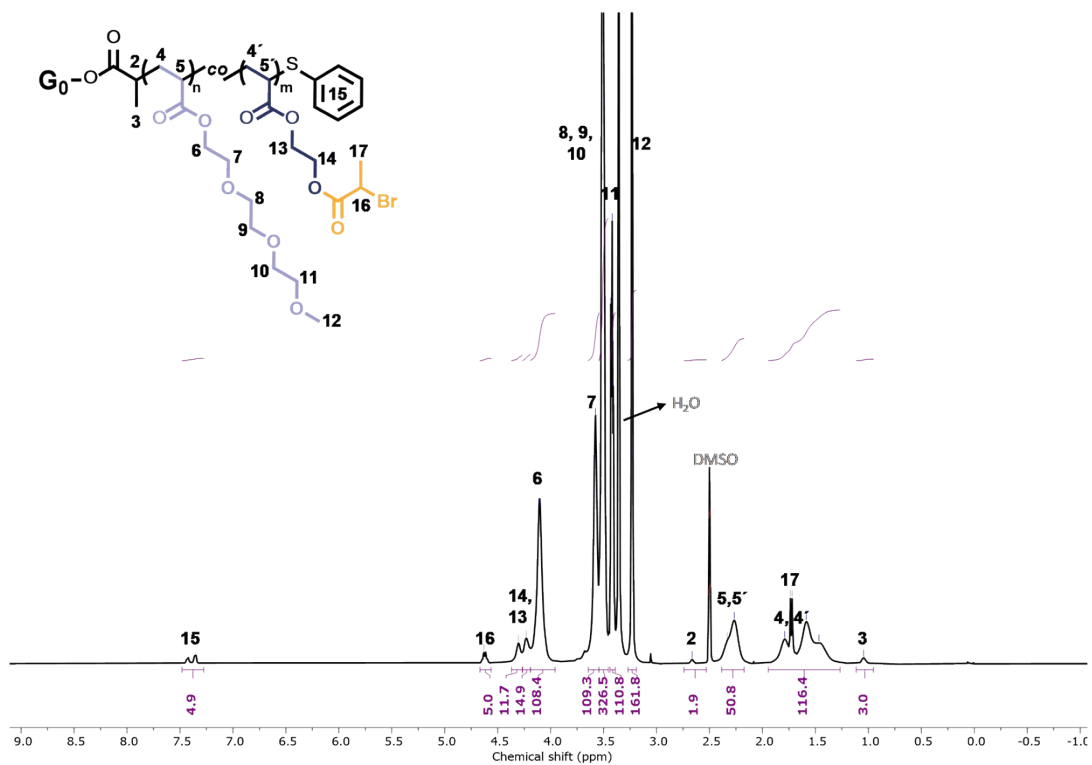


Figure S6.  $^1\text{H-NMR}$  of  $\text{G}_0$ -poly(TEGMEA-co-HEA) with  $DP = 49$ ,  $M_w^{\text{SLS}} = 330 \text{ kg}\cdot\text{mol}^{-1}$  and  $\mathcal{D} = 1.11$ .

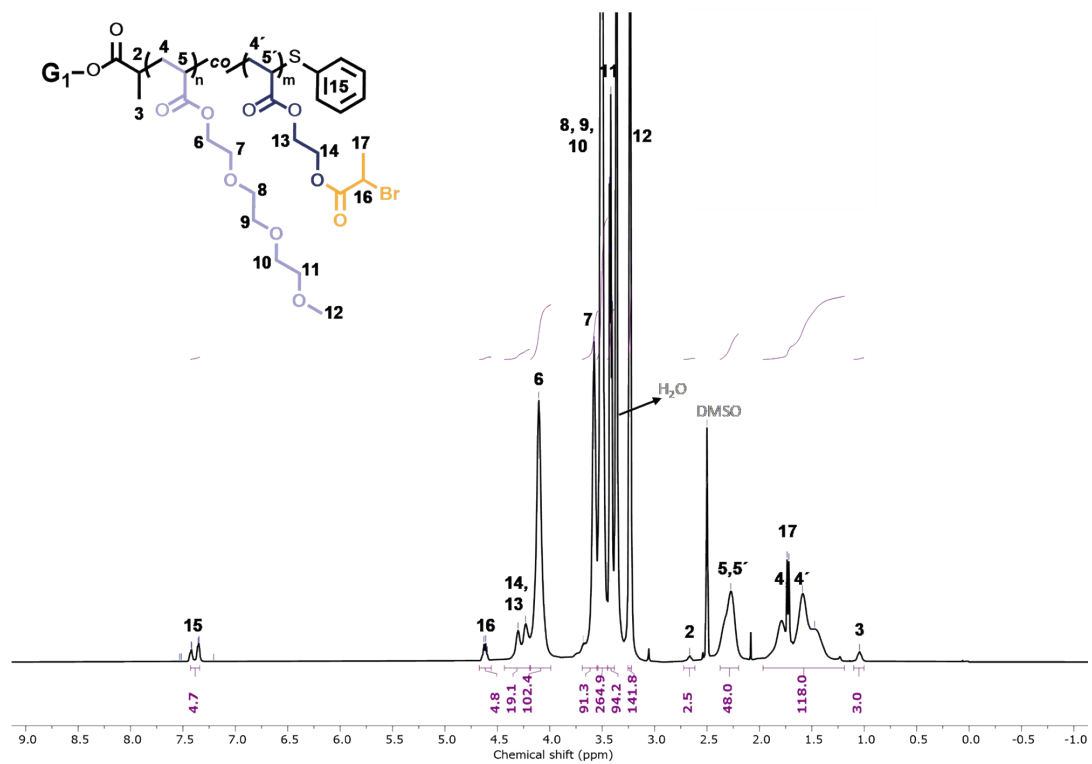


Figure S7.  $^1\text{H-NMR}$  of  $\text{G}_1$ -poly(TEGMEA-co-HEA) with  $DP = 45$ ,  $M_w^{\text{SLS}} = 1400\text{-kg}\cdot\text{mol}^{-1}$  and  $\mathcal{D} = 1.17$ .



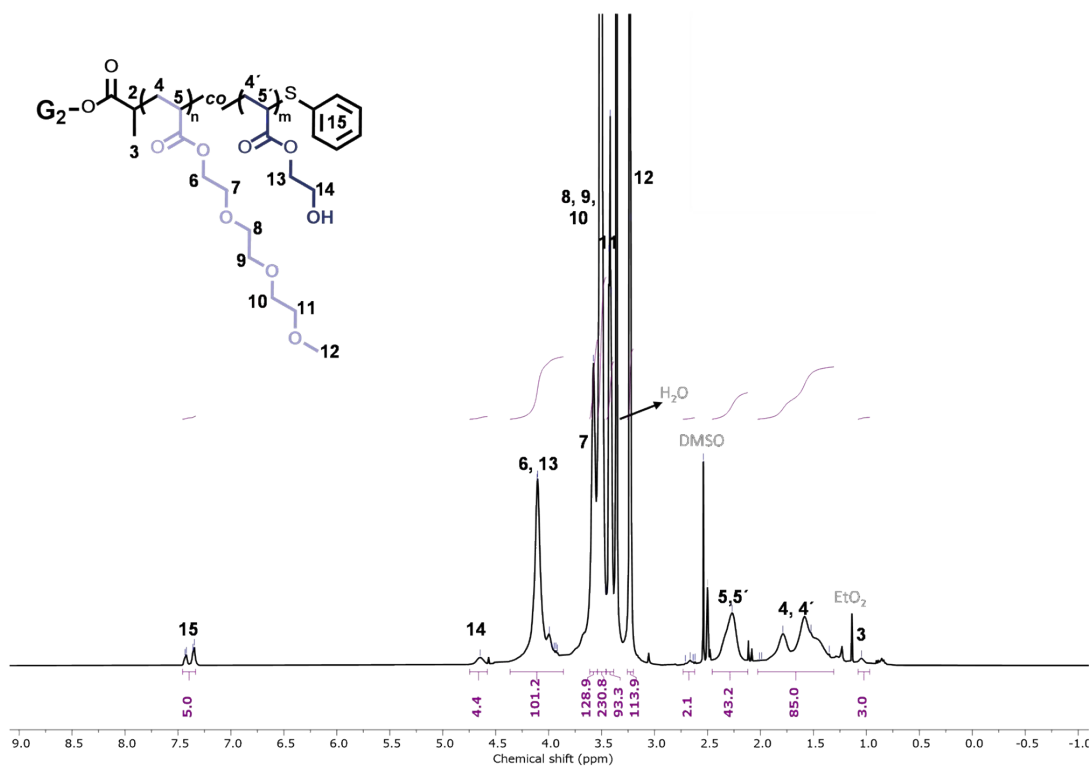
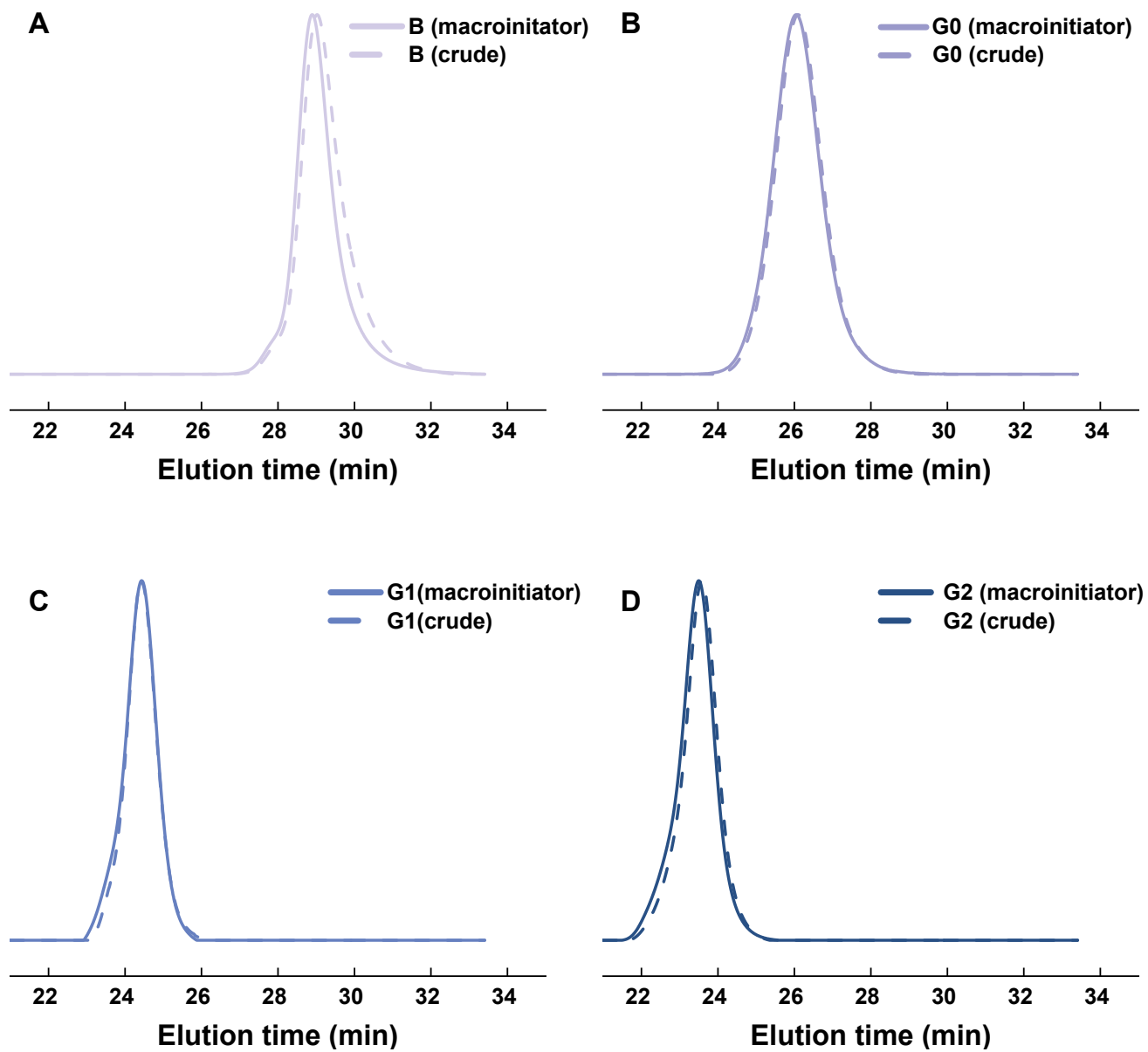


Figure S8. <sup>1</sup>H-NMR of G3 poly(TEGMEA-co-HEA) with  $DP = 46$ ,  $M_w^{SLS} = 6200 \cdot \text{kg} \cdot \text{mol}^{-1}$  and EGF of >99%.

SEC-Elution profiles backbone to G2



**Figure S9.** SEC-elution profiles for the crude polymerization mixture (dashed line) and the final purified macroinitiator (solid line) for (A) linear backbone, (B) G0, (C) G1 and (D) G2 demonstrating that the purification steps do not influence the molecular weight distribution.

### Molecular weight determination by static light scattering

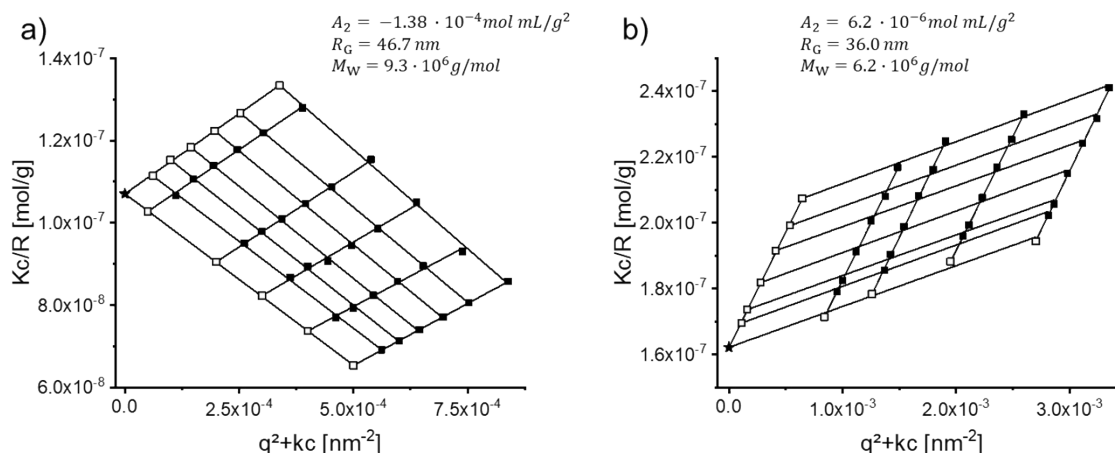


**Figure S10.** Zimm plots of G3 in a) water and b) in THF, respectively measured at 25°C. The higher values for the molecular weight  $M_w$  and the radius of gyration  $R_G$  in water compared to THF presumably arise from a weak aggregation tendency of G3 in water, which is further supported by the negative second virial coefficient  $A_2$  that indicates an attractive pair potential between G3 in aqueous solution.

### Characterization of the arborescent structure in solution

The hydrodynamic radius ( $R_h^{\text{DLS}}$ ) of the different arborescent generations G0-G3 was measured in dilute solutions in water (Table 1, main manuscript) and THF by dynamic light scattering (DLS) and compared to the  $R_h^{\text{DPD}}$  obtained from the density profiles and displayed in Figure S11.

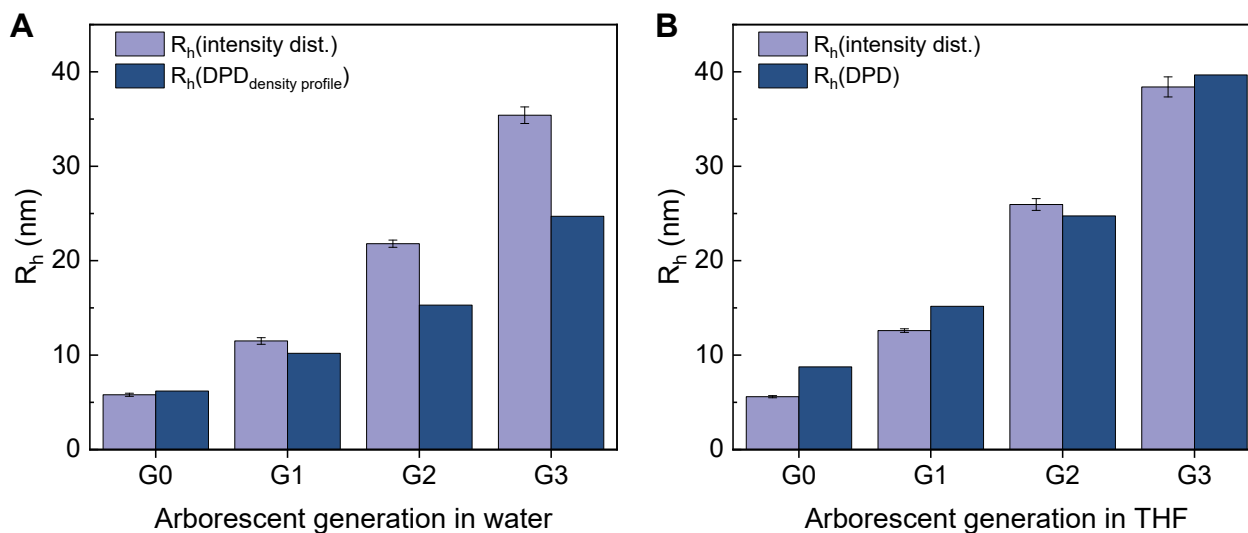


**Figure S11** Comparison of the hydrodynamic radii of arborescent poly(TEGMEA-co-HEA) obtained from DLS (intensity distribution) and DPD simulation. A: in water, B: in THF

### Characterization of the arborescent structure at the solid-air interface

The AFM height images were evaluated to evaluate the deformability based on the the vertical compression, as the ratio of the height at the interface to the hydrodynamic diameter  $VC_{int} = h_{2D}/(2 \cdot R_h)$  and lateral spreading using the softness parameter which is the ratio of the radius at the interface to the hydrodynamic radius in solution ( $S_{int} = R_{2D}/R_h$ ). Figure S12 shows the height  $h_{2D}$  at the interface for the two observed conformations disc-like (A) and fried-egg (B). Since the shape of the individual adsorbed polymers diverged from a spherical shape the softness parameter was calculated from the area at the surface  $A_{2D}$  obtained from the AFM height image analysis described above based on the following relationship:

$$S_{int} = \frac{R_{2D}}{R_h} = \sqrt{\frac{A_{2D}}{\pi \cdot R_h^2}} \quad (17)$$

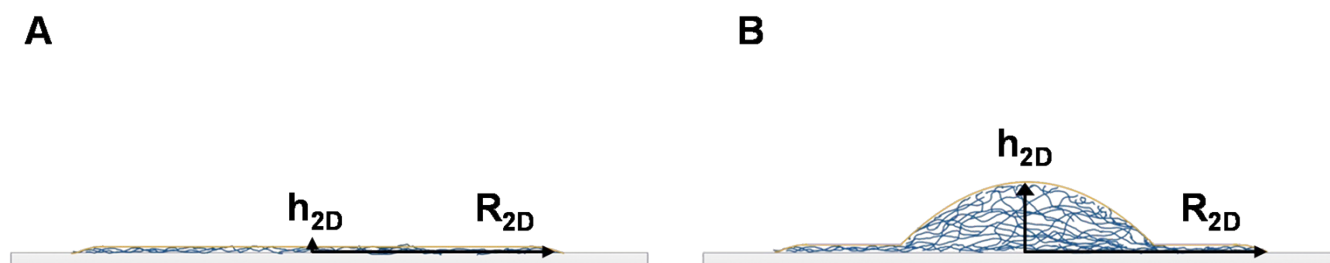


**Figure S12** Schematic representation of the two observed surface conformations including (A) disc-like and (B) fried-egg.

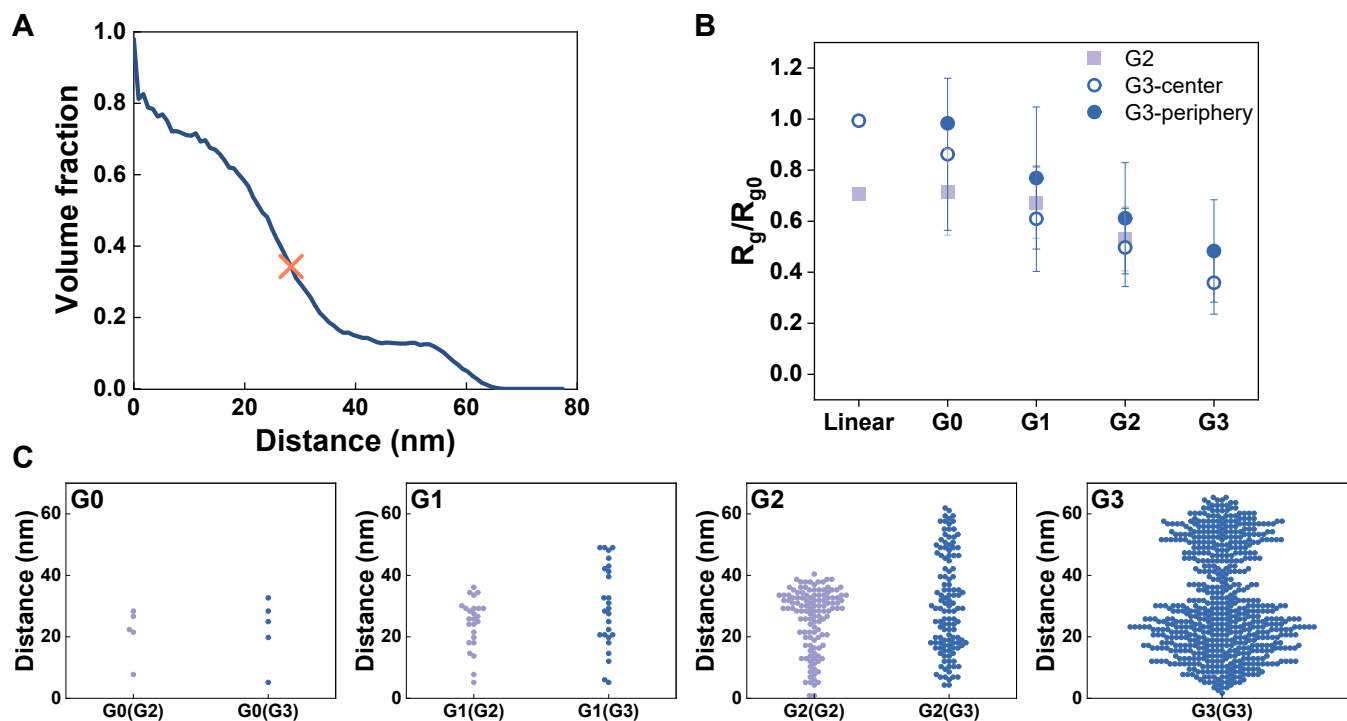


**Figure S13** (A) Cylindrical density profile of G3-poly(TEGMEA-co-HEA) adsorbed at the solid interface. The orange cross denotes the inflection point of the second decrease, which was chosen as border between the center and the flat periphery of the molecule. (B) Ratio of the radii of gyration of the adsorbed backbones of the individual generations inside of the G2 and G3 arborescent polymer and the corresponding  $R_g$  for a rod polymer ( $R_g/R_g^{rod}$ ), G3 is divided into two regions G3-center and G3-periphery (C) (E) Position of the end-groups as distance from the center of mass in each individual generation extracted from the G2 polymer (light purple) and the G3 polymer (blue). Each data points represents one end group

## Characterization of the arborescent structure at the liquid-liquid interface

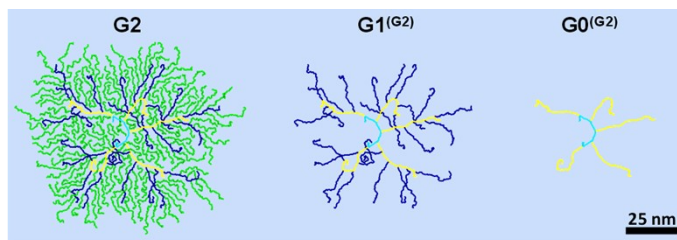


**Figure S14** DPD simulation snapshots of G2 poly(TEGMEA-co-HEA) at the oil-water interface, top view of the adsorbed G2 molecule represented by the acrylate backbone only without side groups. From the simulated G2 molecule, G1 and G0 are extracted and visualized individually. Scale bar equivalent to 25 nm for all images.

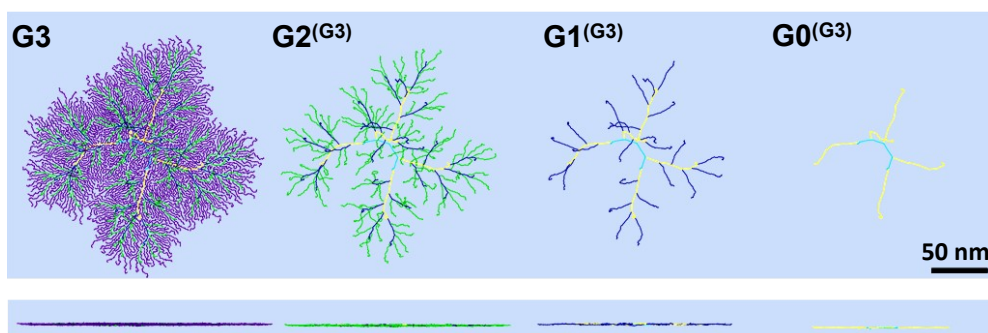


**Figure S15** DPD simulation snapshots of G3 poly(TEGMEA-co-HEA) at the oil-water interface, top and side view of the adsorbed G3 molecule represented by the acrylate backbone only without side groups. From the simulated G3 molecule, G2, G1 and G0 are extracted and visualized individually. Scale bar equivalent to 50 nm for all images.

Figure S16 shows additional AFM height images of the adsorbed polymer layer deposited on silicon wafers at the different surface pressures during compression of the interface. Images in Figure S16D were used to calculate the relative grain area as well as the height of the grains.

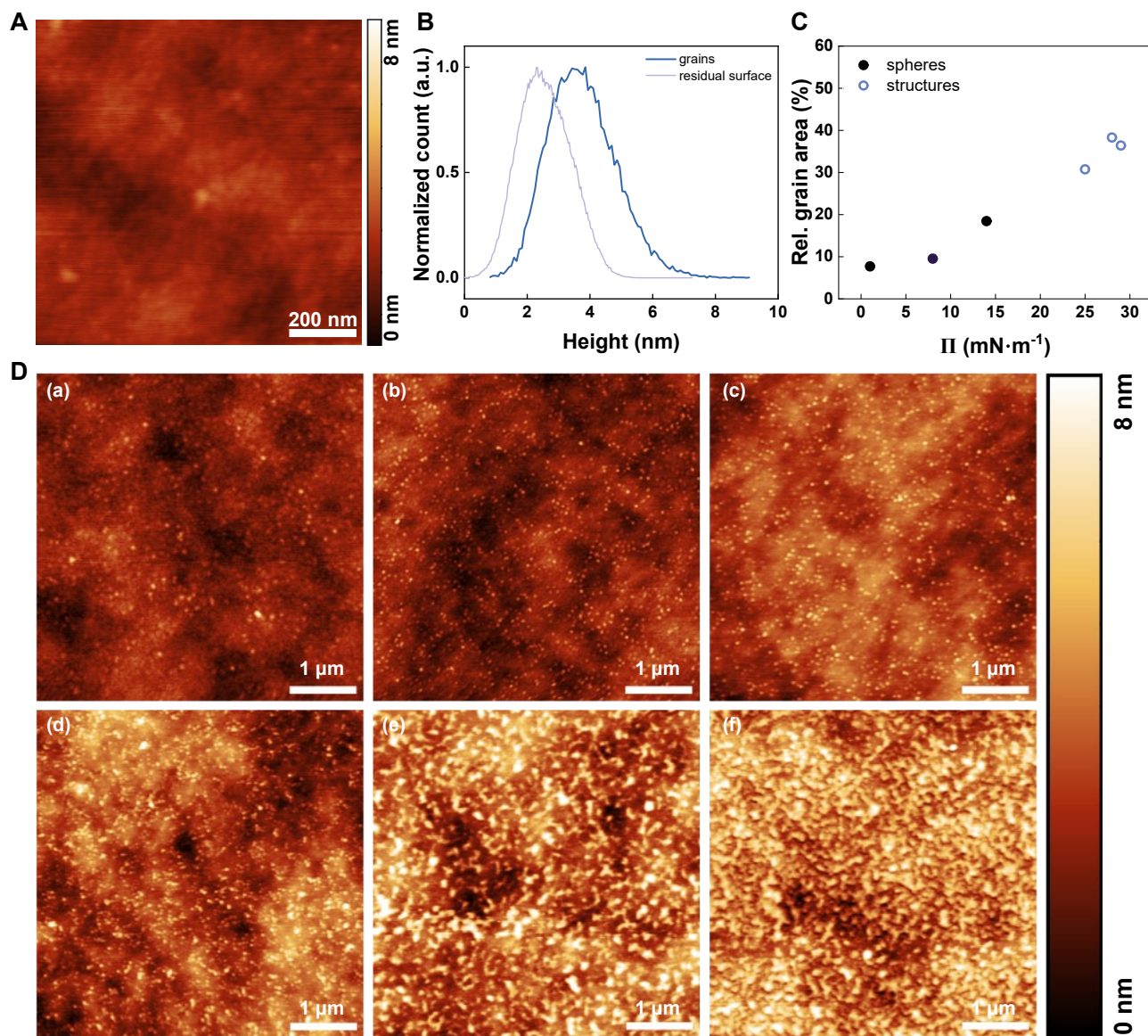


**Figure S16** (A) AFM-height micrograph of a grain-free area at low compression at  $\Pi = 1 \text{ mN}\cdot\text{m}^{-1}$ , corresponding to point (a) of the compression isotherm (B) Exemplary height distribution of the grains and the residual surface at  $\Pi = 8 \text{ mN}\cdot\text{m}^{-1}$ , corresponding to point (c) of the compression isotherm (C) Relative area covered by grains at different surface pressures. Data points correspond to the  $5 \times 5 \mu\text{m}$  height images shown in (D). (D) AFM height images of the deposited polymer layers in the dry state (scale  $5 \times 5 \mu\text{m}$ ). The position of the images (a)-(f) are highlighted in the compression isotherm in the main manuscript.

### 3. Literature

1. M. Hoorfar and W. N. A, *Adv Colloid Interface Sci*, 2006, **121**, 25-49.
2. G. Kretzschmar, R. Miller and S. S. Dukhin, *Dynamics of Adsorption at Liquid Interfaces*, 1995.
3. C. M. Hansen, *Hansen Solubility Parameters*, Taylor&Francis Group, Boca Raton, Second Edition edn., 2007.
4. T. Lindvig, M. L. Michelsen and G. M. Kontogeorgis, *Fluid Phase Equilibria*, 2002, **203**, 247-260.
5. A. A. Gavrilov, W. Richtering and Potemkin, II, *J Phys Chem B*, 2019, **123**, 8590-8598.
6. Y. Li, M. Kröger and W. K. Liu, *Nanoscale*, 2015, **7**, 16631-16646.
7. H. Lee, A. H. de Vries, S.-J. Marrink and R. W. Pastor, *The Journal of Physical Chemistry B*, 2009, **113**, 13186-13194.
8. A. P. Thompson, H. M. Aktulga, R. Berger, D. S. Bolintineanu, W. M. Brown, P. S. Crozier, P. J. in 't Veld, A. Kohlmeyer, S. G. Moore, T. D. Nguyen, R. Shan, M. J. Stevens, J. Tranchida, C. Trott and S. J. Plimpton, *Computer Physics Communications*, 2022, **271**.
9. L. Hoppe Alvarez, S. Eisold, R. A. Gumerov, M. Strauch, A. A. Rudov, P. Lenssen, D. Merhof, Potemkin, II, U. Simon and D. Woll, *Nano Lett*, 2019, **19**, 8862-8867.
10. G. Del Monte, D. Truzzolillo, F. Camerin, A. Ninarello, E. Chauveau, L. Tavagnacco, N. Gnan, L. Rovigatti, S. Sennato, E. Zaccarelli. *Proc. Natl. Acad. Sci. U. S. A.* **2021**, 118, No. e2109560118.